

Standing shocks in a rotating channel

Tivon E. Jacobson^{a)}

Department of Earth and Planetary Sciences, The University of Tokyo, 7-3-1 Hongo, Bunkyo-ku, Tokyo 113-0033, Japan

Esteban G. Tabak^{b)}

Courant Institute of Mathematical Sciences, New York University, 251 Mercer Street, New York, New York 10012

(Received 5 June 2003; accepted 15 June 2004)

This paper discusses the stationary shallow water shocks occurring in a reentrant rotating channel with wind stress and topography. Asymptotic predictions for the shock location, strength, and associated energy dissipation are developed by taking the topographic perturbation to be small. It is shown that under appropriate conditions, a mean flow develops under the action of the wind stress, with a transverse profile determined by the need to support stationary shocks. The scaling arguments for the asymptotics are developed by demanding integrated energy and momentum balance, with the result that the free surface perturbation is of the order of the square root of the topographic perturbation. Shock formation requires that linear waves be nondispersive, which sets a solvability condition on the mean flow and which leads to a class of generalized Kelvin waves. Two-dimensional shock-resolving numerical simulations validate the asymptotic expressions and demonstrate the presence of stationary separated flow shocks in some cases. © 2004 American Institute of Physics. [DOI: 10.1063/1.1780172]

I. INTRODUCTION

A major problem in atmospheric and oceanic study is the effective parametrization of wave breaking and energy removal processes. In some contexts, one may wish to resolve carefully the wave breaking. However, in other cases, it would be progress to simply install in a model the gross features of wave breaking—energy loss (via transfer to unresolved scales), generation of vorticity, or sudden changes in velocity, pressure, or other thermodynamic variables across the breaking region. For example, this was done by Bühler and Jacobson using shallow water shocks for the case of wave breaking on a beach, in an attempt to understand the generation of longshore currents shoreward of a sandbar.¹

The shallow water equations (SWEs) are a prime candidate for certain models of gravity wave breaking: they support gravity waves and are ubiquitous in geophysical studies. In one guise or another, they appear as the governing equations for the barotropic and baroclinic modal decompositions of the atmosphere and ocean. The formation of shocks in shallow water gravity waves may be taken as a gross model of the three-dimensional wave breaking of barotropic waves. However, this is rarely done in large-scale geophysical applications, probably because of the dispersive effect of rotation and mean currents on gravity waves, which inhibit shock formation. There is, however, an exceptional case: the nondispersive Kelvin wave. Since these waves require boundaries of some kind, they are typically present in the atmosphere as equatorially trapped Kelvin waves. The ocean

can support Kelvin waves at midlatitudes and polar latitudes as well, due to the presence of physical boundaries.

In this paper we explore the role of a generalized version of breaking Kelvin waves in a reentrant f -plane channel. These solutions balance energy input from wind stress with energy dissipation at shocks. All the energy dissipation must be by means of a shock, since no explicit dissipation is included in the model.

Our focus is on stationary solutions with stationary shocks, although transient shock generation is more likely to be of interest in applications of the SWE to real geophysical flow. This is because stationary shocks must arise from the nonlinear deformation of waves with speeds of the same order as the mean flow, so that the two speeds cancel out. On large scales in the ocean, this mean flow speed rarely exceeds 20 cm/s. For stationary shocks, we must then have wavespeeds c of the same order. The corresponding Rossby radii are of order $c/f \sim 2000$ m in midlatitudes. This scale is probably too small for the decoupling of the interior (eddy induced) viscous shock structure from rotational effects: the width of the shock may not be small compared with a Rossby radius. Furthermore, the wavespeed is much too low for the barotropic or first baroclinic mode: the stationarity could only arise for wave propagation in higher baroclinic modes.

Certain dense sill overflows have flow velocities of around 1 m/s—high enough to match the appropriate principal baroclinic wavespeed—but we have not found a way to apply to that case the asymptotic methods of the periodic channel theory in this paper. A literature on the role and structure of shocks in a nonperiodic rotating channel with known upstream or initial conditions exists. Unlike the theory presented by Gill,² which does not explicitly consider

^{a)}Tel: +81-3-5841-4294; FAX: +81-3-5841-8791; Electronic mail: tivon@eps.s.u-tokyo.ac.jp

^{b)}Tel: 1-212-998-3088; FAX: 1-212-995-4121; Electronic mail: tabak@cims.nyu.edu

the shock matching problem, such investigations have had to overcome hurdles associated with near shock boundary layers and the nonconservation of potential vorticity at the shock. Advances have been made through various specializations. For example, Nof considered particular cross-channel shock structure,³ while Fedorov and Melville tackled weak shocks and strong shocks with weak cross-channel flow.⁴ Helfrich *et al.*⁵ and Pratt *et al.*⁶ made progress by computing numerical solutions and using these to verify previous predictions and to identify new flow features.

Our asymptotic calculation begins with an undetermined zero-order flow field in geostrophic balance. The zero-order flow field is determined up to a single parameter by the requirement that the linearized equations support nondispersive waves. In our model, this parameter is fixed by the requirement of stationarity. The remainder of the work is in determining the linearized flow field from solvability conditions at higher order.

The results are the description of a family of nondispersive generalized Kelvin waves and an asymptotic theory for stationary shocks in the presence of moderate rotation and weak forcing. The asymptotic theory is checked against numerics from a two-dimensional shock-resolving shallow water solver, with good agreement. The solver uses a second-order Godunov-type method, and was spun up by the wind stress to the forced-dissipative steady state. In addition to checking the numerics for moderate rotation, we include numerical results relating to stationary shocks in the presence of strong rotation. We found that stationary states were achieved for rotations outside the domain of applicability of the asymptotic theory. Notably, stationary states were observed even when the rotation became large enough to separate the flow from one side of the channel.

This model was originally motivated as a rotational extension of the work of Goldak and Tabak,⁷ who made a toy nonrotating forced-dissipative model to explain momentum and energy balance in the antarctic circumpolar current (ACC). We have already mentioned that the model in this paper is probably not directly relevant to the ACC, at least not without further refinements, because of the flow magnitudes involved. It is also missing some key physics, most notably baroclinic effects, although these were handled by Goldak for the nonrotating case.⁷ On the other hand, it provides and validates a formal asymptotic theory in which the structure of a mean flow is related to higher-order forcing and dissipation, a central problem in geophysical fluid dynamics. Our model also recognizes that the wind stress is an energy input to a moving current and that the energy must be dissipated somewhere. In this paper the energy is dissipated at the shock, which also happens to be responsible for wind stress/form drag balance in the steady state. This was a prime motivation for its original use as a toy model of the ACC—it illustrates that arguments which give the flow strength of that current by momentum balance but which do not properly account for energy dissipation may not be viable.

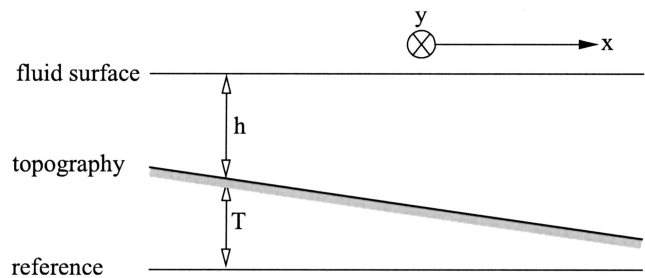


FIG. 1. SWE: Definition of variables and configuration.

II. THE SHALLOW WATER EQUATIONS

The SWEs may be derived from the three-dimensional, finite-depth, irrotational, constant density fluid equations in the limit of small depth to horizontal length ratio.^{8–12}

In the presence of rotation, topography, and forcing they are (see also Fig. 1)

$$(h\vec{u})_t + \nabla \cdot (h\vec{u} \otimes \vec{u}) + g \nabla \cdot \left(\frac{h^2}{2} \right) + fh\vec{u}^\perp = -gh \nabla T + \vec{w}, \quad (1)$$

$$h_t + \nabla \cdot (h\vec{u}) = 0. \quad (2)$$

The first equation is the depth-integrated momentum equation, and \vec{u} is the two-component vector of depth-integrated horizontal velocities. The terms in $\nabla h^2/2$ and $h \nabla T$ arise from enforcement of the lower and upper boundary conditions in the derivation of the equations. The fluid depth h acts like a density in the SWE, and so there is an effective pressure with equation of state $p = gh^2/2$, and a form drag $gh \nabla T$, where T represents the bottom topography. The notation \vec{u}^\perp is meant to indicate the two horizontal space components of the velocity \vec{u} rotated counterclockwise by 90° . In the Northern Hemisphere, the Coriolis parameter f is positive. The constant g is the gravity (or possibly, the reduced gravity), and \vec{w} is the vector stress, distributed uniformly through the thickness h of the fluid. Unfortunately, the shallow water model does not support any variations with the vertical coordinate, so the concept of a vertically uniform stress leads to difficulties in the event that the layer depth h tends to zero (Sec. IX).

These equations are in conservation form, which means that in the absence of forcing terms (here, we also mean $f = 0$ and no topographic form drag), the integrals over a periodic domain Ω are conserved,

$$\frac{d}{dt} \int_{\Omega} h\vec{u} \, dS = 0, \quad (3)$$

$$\frac{d}{dt} \int_{\Omega} h \, dS = 0. \quad (4)$$

Also in the absence of forcing, all change in the local volume integrals of $h, h\vec{u}$ must come from fluxes through the local boundaries.

It is completely typical that the solutions form shocks in finite time. Therefore, discontinuous solutions of the equa-

tions must be allowed, and the appropriate equations are the weak form of (1) and (2). However, no confusion need be caused as long as the conservation form is remembered in all cases where the solution may be nonsmooth. In smooth regions of the flow, there is an energy which is conserved, but this energy always decreases in the direction of flow across admissible shocks. Derivation of this energy E follows from taking the inner product of (1) with \vec{u} and using mass conservation to obtain

$$\left(h \frac{|\vec{u}|^2}{2} + g \frac{h^2}{2} + ghT \right)_t + \nabla \cdot \left[\vec{u} \left(h \frac{|\vec{u}|^2}{2} + gh^2 + ghT \right) \right] = \vec{w} \cdot \vec{u}. \quad (5)$$

The energy E is therefore the quantity under the time derivative.

A. Scaling

In this paper, we will be discussing flows in a periodic channel with characteristic width L . The usual procedure for nondimensionalizing the shallow water equations is to take $c_0 = \sqrt{gH}$, where H is a characteristic depth of the fluid, and replace

$$\vec{u} \leftarrow c_0 \vec{u}',$$

$$(x, y) \leftarrow L(x', y'),$$

$$t \leftarrow \frac{L}{c_0} t',$$

$$h \leftarrow Hh',$$

$$T \leftarrow HT',$$

$$f \leftarrow \frac{c_0}{L} f',$$

$$w \leftarrow \frac{c_0^2 H}{L} w'.$$

The equations are now being solved in a channel of unit width, unit characteristic depth and unit linear wavespeed. They read

$$(h\vec{u})_t + \nabla \cdot (h\vec{u} \otimes \vec{u}) + \nabla \cdot \left(\frac{h^2}{2} \right) + fh\vec{u}^\perp = -h \nabla T + \vec{w}, \quad (6)$$

$$h_t + \nabla \cdot (h\vec{u}) = 0, \quad (7)$$

where the primes have been dropped. The remaining parameters and parametric functions are the nondimensionalized f , T , and w . Note that the nondimensional f is the ratio of channel width to deformation radius. All of our results are presented in these terms.

B. Linear waves

We consider first linear unforced waves on a motionless background state of unit depth in an unbounded domain. For linearized theories, shocks do not form, and we may drop the conservative form

$$\vec{u}_t + \nabla h + f\vec{u}^\perp = 0, \quad (8)$$

$$h_t + \nabla \cdot \vec{u} = 0. \quad (9)$$

Without rotation, this is a nondispersive linear wave equation for surface gravity waves. In the presence of rotation, the linear waves are modified. A substitution of plane wave solutions

$$e^{i(kx - \omega t)}$$

into the equations yields the dispersion relation

$$\omega(\omega^2 - k_1^2 - k_2^2 + f^2) = 0.$$

Aside from the vortical waves ($\omega=0$), this equation has the dispersive Poincaré wave solutions

$$\omega = \pm \sqrt{k_1^2 + k_2^2 - f^2}. \quad (10)$$

It is also, in the presence of a boundary along $x=0$, say, permissible to take $k_2 = \pm if$. The result is that a family of nondispersive Kelvin waves appear: $\omega = \pm k_1$. It is also necessary that the cross-boundary component of the velocity be zero in this case, otherwise the Kelvin waves cannot satisfy the very boundary conditions which sustain them. The choice of sign for k_2 depends on whether the flow domain is a channel, an upper half plane, or a lower half plane. In the Northern Hemisphere, the exponentially trapped waves travel with the boundary on their right.¹⁰

If the depth of the water column is not uniform, the linearized equations do not have constant coefficients. The linear wavespeed c_0 will vary with position. A nonconstant background flow may also be present (as in the linearized geostrophically balanced rotating system) which contains terms like $u^0(\vec{x})u^1$ (advection of the wave field u^1 by the background). Although it appears that nondispersive waves will no longer be present, we will return to this point in Sec. V, where a special class of nondispersive waves will be exhibited.

C. Shocks

At finite wave amplitudes, nonlinearity causes the nondispersive wave profiles to form shocks.

By examining the properties of discontinuous solutions in the weak (integral) form, one obtains the Rankine-Hugoniot equations which relate shock propagation speeds to the ratio of the jumps in flux and conserved quantity across the shock (denoted by $[\cdot]$). Regardless of the presence or absence of rotation, the jump conditions have the same form, as the undifferentiated terms have no effect on the Rankine-Hugoniot relations. For a shock which is crossed normally by the component u_n of \vec{u} (the other component being u_t),

$$-s[hu_n] + \left[hu_n^2 + \frac{h^2}{2} \right] = 0, \quad (11)$$

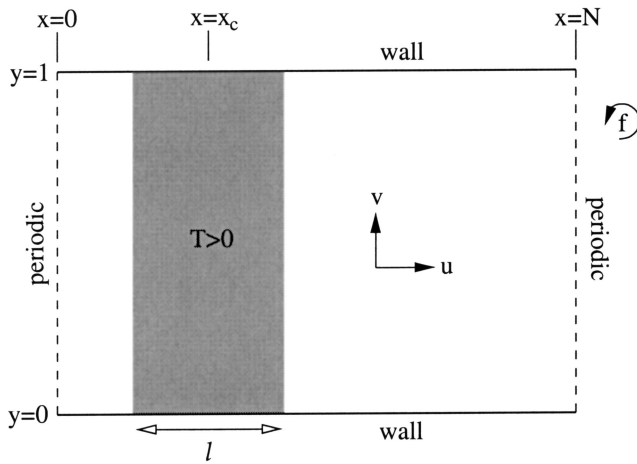


FIG. 2. The channel model (plane view).

$$[u_t] = 0, \quad (12)$$

$$-s[h] + [hu_n] = 0. \quad (13)$$

Here, s denotes the speed of the shock.

There is a further result with which we will make contact. It is possible to write down the rate of energy production \dot{E} at a *stationary* shock. It is always less than zero for admissible shocks,¹³

$$\dot{E} = -\frac{u_{n,1}[h]^3}{4h_2} \quad (14)$$

$$= -\frac{u_{n,2}[h]^3}{4h_1}. \quad (15)$$

Here, $u_{n,1}$ is the upstream normal component of \vec{u} , and $u_{n,2}$ the downstream normal component. The quantities h_1 and h_2 are the fluid depths before and after the shock (following a fluid particle).

III. CHANNEL MODEL

Figure 2 presents the channel model we use throughout this paper. After suitable scaling (Sec. II A) it is a channel of width 1 and some length N . (We have $N=2$ in all numerical simulations.) The characteristic depth scale is also 1. We refer to the x (along channel) component of the velocity as u , and the y (cross channel) component as v . Along channel can be distinguished from cross channel by periodicity in the along-channel direction and by the reflecting walls at $y=0$ and $y=1$. The direction of the applied wind stress is along channel, and the topography varies only with the along-channel coordinate x ,

$$(hu)_t + (huu)_x + (hvu)_y - fhv + \left(\frac{h^2}{2}\right)_x = -hT_x + w, \quad (16)$$

$$(hv)_t + (huv)_x + (hvv)_y + fhu + \left(\frac{h^2}{2}\right)_y = 0, \quad (17)$$

$$h_t + (hu)_x + (hv)_y = 0. \quad (18)$$

In the model, whenever topography is present, it will be a squared cosine over one arch of the cosine function,

$$T(x) = \begin{cases} T_m \cos^2\left[\frac{\pi}{2l}(x-x_c)\right] & \text{if } |x-x_c| < l \\ 0 & \text{otherwise.} \end{cases} \quad (19)$$

The center of this bump is at x_c and it has width l .

It remains only to specify the initial values of u , v , and h . We take u, v to be zero initially, and h to be such that $h + T$ is constant throughout the channel, and with some specified mass M ,

$$\int_0^1 \int_0^N h \, dx \, dy = M.$$

Typically, h will be about 1, so that $M \sim N$.

IV. CRITICAL NONDISPERSIVE GEOSTROPHIC FLOW

It is possible to guess the attributes of a steady flow from the configuration of the problem. First, any steady flow must include a shock to dissipate the energy input by wind forcing. For a stationary shock, this implies that the flow must be supercritical upstream of the shock and subcritical downstream. Since the domain is periodic, it follows that the flow will pass smoothly from subcriticality to supercriticality somewhere. Second, for weak shocks, the flow deviates only slightly from a zonal flow; this means that the mean flow in the weak shock problem is in cross-channel geostrophic balance. These two conditions dictate the general structure of the mean flow field: geostrophic balance by itself allows many solutions for the mean flow, but the additional requirement of transcriticality selects the unique solution for the mean flow field which allows for a stationary shock. We will see this in more detail when we consider that waves on the mean flow must be nondispersive (Sec. V). It should be noted that the scaling that results for weak wind forcing is the usual scaling of semigeostrophic theory. In contrast with some approaches to obtaining the semigeostrophic scaling, we start with the assumption of weak wind forcing and steady flow rather than a channel geometry whose along-channel length scale is much greater than its cross-channel length scale.

Since the forced-dissipative structure of the problem determines the mean flow, the solution for the structure of the flow field differs from that obtained in some other instances of semigeostrophic flow in a channel.² It is more usual to consider semigeostrophic flow in a channel which originates in a basin upstream. In that case, the flow is not really in forced-dissipative equilibrium in the domain, for imbalances in the energy and momentum budget may be accommodated through upstream and downstream boundary fluxes. The mean flow is determined by the complementary conditions of cross-channel geostrophic balance and known potential vorticity upstream. These models are of prime importance in a variety of hydraulically controlled oceanic phenomena involving sill overflows and the communication of ocean basins through narrow straits. However, shock fitting is difficult

in these cases since the change in potential vorticity across a variable-strength shock is nonuniform, and it is not necessary that the flow is in geostrophic balance in the immediate vicinity of the shock. The boundary layers which adjust the flow to geostrophic balance following disruption by the shock are much wider than the shock itself and it is difficult to see how mass and momentum balance can be applied across these layers. Fedorov and Melville solved for the structure of shocks propagating into an undisturbed fluid in a semigeostrophic channel with their associated boundary layers.⁴ Recent numerical studies of shocks in a semigeostrophic channel with known upstream boundary conditions have done much to confirm and further elucidate the structure of these shocks as well as the role they play in hydraulic control and adjustment.^{5,6}

Let us now explain, step by step, the procedure by which the asymptotic solution for the flow field is determined in the periodic forced-dissipative case. The first step is the determination of the asymptotic structure of the flow fields and the relationship between the size of the topography and the wind stress. Consider the integrated momentum and energy balances [from (16) and (14), respectively],

$$\int_0^1 \int_0^N w - hT_x dx dy = 0, \quad (20)$$

$$\int_0^1 \int_0^N wu dx dy \sim [h]^3. \quad (21)$$

We may as well assume that the shock occurs at first order in the depth field, that is,

$$h = h^0(y) + \epsilon h^1(x, y) + O(\epsilon^2). \quad (22)$$

Since the flow is somewhere transcritical, it follows from the conservation equations that the velocity field has the same asymptotic structure,

$$u = u^0(y) + \epsilon u^1(x, y) + O(\epsilon^2). \quad (23)$$

We will see later that the cross-channel velocity field vanishes at zeroth and first order. (§) Using this information, we obtain from (21) the asymptotic scaling for w ,

$$Nwu^0 \sim \epsilon^3 \Rightarrow w \sim \epsilon^3. \quad (24)$$

Since T_x has mean zero, (20) may be recast as

$$\epsilon^3 \sim Nw \sim \int_0^1 \int_0^N (h - h^0)T_x dx dy \sim \epsilon NT_x. \quad (25)$$

The asymptotic scaling for the topography is $T \sim \epsilon^2$. [In later sections we have estimated ϵ for presentation along with the results of numerical experiments. There we put $\epsilon = \sqrt{T_m}$ with T_m the maximum value of the topography. It may be argued that this underestimates ϵ in view of the order 1 factors which are present in (25). However, the nature of ϵ is always approximate in an asymptotic theory, and it does not affect the form of the solution as long as it is used consistently.] In this derivation, we have ignored the effect of the changing strength of the shock across the channel, but this is not expected to affect these order of magnitude estimates. This

turns out to be legitimate, as can be seen by comparison of the theory with numerical results. So far, we have made no reference to the width of the channel, and the same asymptotic scalings apply to a nonrotating, one-dimensional flow.⁷

The next step is to consider mean flow fields which allow stationary nondispersive waves in the linearized (first-order) equations. It is only when nonlinearity acts on nondispersive waves that shock formation is expected. Perhaps not surprisingly, the condition on the mean flow is criticality (Sec. V),

$$u^0(y) = \sqrt{h^0(y)}. \quad (26)$$

That is, to say, the mean flow is a transcritical flow at each value of the cross-channel coordinate. In the one-dimensional nonrotating case, incidentally, this still applies, but there is only one cross-channel coordinate to consider! In fact, the presence of rotation appears only in the cross-channel geostrophic balance condition. Together, cross-channel geostrophic balance and mean flow criticality determine the mean flow up to a constant of integration. The constant of integration is determined by the total mass content of the channel, which we are free to set as an initial condition.

The mathematical determination of the first-order flow field is a little more involved, but the steps are again straightforward. Cross-channel geostrophic balance is still present at first order. This allows the wave field variables u^1 and h^1 to be related. The equations reduce to a single equation for, say, h^1 . This equation is not constant coefficient, but as the coefficients depend only on the cross-channel coordinate, it may be integrated along the channel. The result is a factored expression for the first-order wave field which contains two unknown functions: one $[d(y)]$ of the cross-channel coordinate, the other $[\mathcal{L}(x)]$ a function of the along-channel coordinate.

It is reasonable at this point that they are unknown functions, for we have not used any information about the structure of the topography or the strength of the wind. The topography appears at second order, and this is precisely what is needed, for we may also apply the usual condition in weakly nonlinear asymptotics that the first-order wave field does not excite any secular terms in the second-order field. Applying this solvability condition determines $\mathcal{L}(x)$ as a multivalued function of the topography, up to a single unknown. This unknown is the shock location x_s , and it determines where $\mathcal{L}(x)$ switches branches: this is the shock. The shock location itself follows from the final piece of information we need to apply: it is determined in the integrated form-drag balance equation from the strength of the wind stress.

What of $d(y)$? Its structure comes from an interesting consideration: conservation of mass and momentum must be explicitly taken into account at the shock. When this is done (Sec. X), we find after considerable manipulation that $d(y)$ is in fact a constant d_0 . It is surprising that so much work is required to show that this function is constant, and it is likely that there is a better way which we have not recognized. In any event, we have the constant d_0 to determine. It can be

found by requiring that the total mass in the first-order field is zero, as it must be, since topography is a second-order quantity and the mass is otherwise accounted for at lowest order.

That is the complete structure of the asymptotic derivation up to the first-order field. The structure of the derivation is parallel in the nonrotating case, with the exception that it is somewhat more straightforward, the mathematics being less complicated in the one-dimensional setting.

A. Asymptotics: No rotation

In this section, we give a brief derivation of the nonrotating asymptotics, after Goldak.⁷ Based on the asymptotic scaling of Sec. IV, we set

$$u = 1 + \epsilon u^1(x) + \epsilon^2 u^2(x) + \epsilon^3 u^3(x) + O(\epsilon^4), \quad (27)$$

$$h = 1 + \epsilon h^1(x) + \epsilon^2 h^2(x) + \epsilon^3 h^3(x) + O(\epsilon^4), \quad (28)$$

and substitute into the nonrotating, one-dimensional flow equations

$$uu_x + h_x = -\epsilon^2 T_x + \epsilon^3 w, \quad (29)$$

$$uh_x + hu_x = 0. \quad (30)$$

By setting $u^0 = \sqrt{h^0} = 1$, we have set the total mass in the periodic domain. The resulting first-order equations are identical, which shows that the zeroth-order terms were chosen correctly,

$$u_x^1 + h_x^1 = 0. \quad (31)$$

We also find that

$$h^1(x) = -u^1(x) - d_0.$$

In the one-dimensional (1D) case, there is no cross-channel structure, and d_0 immediately emerges as a constant. Moreover, the role of $\mathcal{L}(x)$ —to which we alluded in Sec. IV—is played in the 1D nonrotating case by $u^1(x)$. At second order,

$$u_x^2 + h_x^2 = -T_x - u^1 u_x^1,$$

$$u_x^2 + h_x^2 = -u^1 h_x^1 - h^1 u_x^1.$$

Subtracting the two equations and substituting for h^1 ,

$$T_x = -\frac{3}{2}[(u^1)^2]_x - d_0 u_x^1$$

which is to say

$$u^1 = \frac{-d_0 \pm \sqrt{d_0^2 - 6(D + T(x))}}{3} \quad (32)$$

for some constants d_0, D . One constant may be determined because u^1 must change branches smoothly at the transcritical point x_t . In fact, it is easy to check from the form of u^1 and h^1 that this change of branches corresponds to a transition from subcriticality to supercriticality. We find that x_t is at the topographic maximum T_m to leading order and that

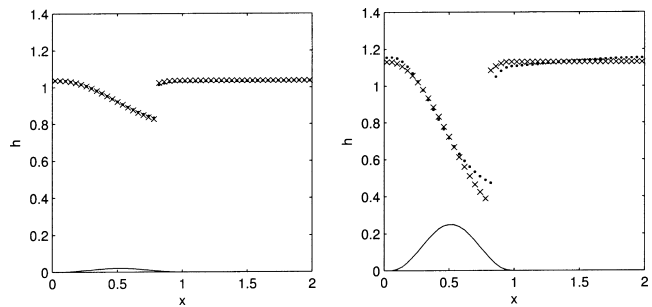


FIG. 3. Asymptotics and numerics, no rotation. On the left is the solution for $T_m=0.02$, $w=0.001$, $\epsilon=0.14$. On the right $T_m=0.25$, $w=0.044$, $\epsilon=0.5$. Here and afterwards, the expansion parameter ϵ is estimated from $\epsilon^2=T_m$. The asymptotic prediction is marked with \times s and the numerical solution with dots. The topography is visible as the solid line at the bottom.

$$d_0^2 - 6(D + T_m) = 0,$$

an equation for D . It must be so: no other choice of x_t would yield an everywhere nonnegative discriminant in (32). We have now

$$u^1 = -\frac{d_0}{3} \pm \sqrt{\frac{2}{3}[T_m - T(x)]}, \quad (33)$$

$$h^1 = -\frac{2d_0}{3} \mp \sqrt{\frac{2}{3}[T_m - T(x)]}. \quad (34)$$

It remains to determine d_0 and the location of the shock. To find the jump location, it is easiest to use the leading expansion term of (20). Denoting the location of the shock as x_s and the location of the topography maximum as x_m ,

$$\begin{aligned} Nw &= -\int_0^N h^1 T_x dx = \pm \int_0^N \sqrt{\frac{2}{3}[T_m - T(x)]} T_x dx \\ &= \int_{x_m}^{x_s} \sqrt{\frac{2}{3}[T_m - T(x)]} T_x dx \\ &\quad - \int_{x_s}^{x_m} \sqrt{\frac{2}{3}[T_m - T(x)]} T_x dx. \end{aligned}$$

This integrates to

$$\frac{Nw}{2} = \left(\frac{2}{3}[T_m - T(x_s)] \right)^{3/2}. \quad (35)$$

Notice that there can be wind stresses so large that no x_s satisfies this equation; in this case, no steady solution is achievable and the forced system will run away.

The constant d_0 is now found by enforcing the first-order mass constraint

$$\int_0^N h^1(x) dx = 0.$$

This constraint on the total mass follows when one recalls that the topography is a second-order quantity.

The solution $1+h^1$ is plotted in Fig. 3 along with a particular choice of topography. A possible direction to take the asymptotics is to compute the higher-order corrections. An

other is to allow the problem to become time dependent, and solve the spin-up problem. One wishes to know whether the steady state we found in the preceding section is reached when wind is applied to some initial configuration. The validity of the results can be checked by solving the PDEs numerically with suitable initial data.

This was done for the nonrotating problem by Goldak and the answer is affirmative, asymptotically and numerically.⁷ A plot of the results of such a numerical spin up appear in Fig. 3 along with the asymptotic solutions. We used the shallow water solver described in Sec. IX. We now turn our attention to the rotating channel.

V. GENERALIZED KELVIN WAVES

One way of viewing the nonrotating hydraulic jump is as a nondispersive gravity wave acted upon by nonlinearity. The upstream (and downstream) propagating waves are advected by the flow. For the stationary case, the advection velocity and the upstream propagation velocity cancel and the gravity waves sit in one place while nonlinearities act. For the shock to develop, the linear wave profile must travel without dispersive distortion.

We expect that the same picture holds for shock formation in the rotating case. If a stationary state is to be present in this model, it must come about via form-drag balance and balance between wind stress energy input and energy dissipation at a shock. However, the only nondispersive waves are the Kelvin waves (Sec. II B), and these are complicated by the presence of a mean flow. The lowest order cross-channel momentum equation is for geostrophic balance,

$$fu^0(y) = -h_y^0(y). \quad (36)$$

The first-order equations are then

$$u_t + u^0(y)u_x - fv = -h_x, \quad (37)$$

$$v_t + u^0(y)v_x + fu = -h_y, \quad (38)$$

$$h_t + u^0(y)h_x + h^0(y)u_x + vh_y^0(y) = 0. \quad (39)$$

Nondispersive waves traveling with speed c satisfy

$$u = U(y)e^{ik(x-ct)},$$

$$v = V(y)e^{ik(x-ct)},$$

$$h = H(y)e^{ik(x-ct)}$$

for all k . Reduction of the equations yields

$$ikU(u^0 - c) - fV = -ikH,$$

$$ikV(u^0 - c) + fU = -H_y,$$

$$ikH(u^0 - c) + kh^0U + h_y^0V = 0.$$

One may use the first equation to eliminate U from the remaining two, leaving a first-order system of ODEs for V, H . Moreover, V must satisfy $V=0$ on $y=0,1$. The problem is an eigenvalue problem for eigenvalues c and eigenfunctions $u^0(y)$. The full range of solutions of the system is unknown

to us. However, taking $V=0$ is one consistent choice, and the origin of our statement that the leading term of the cross-channel velocity is $O(\epsilon^2)$. It has the virtue of rendering the problem simple and of consistency with numerical results.

Eliminating U and setting $V=0$, we obtain

$$(u^0 - c)H_y = fH \quad (40)$$

and

$$\frac{h^0}{(u^0 - c)}H_y = fH, \quad (41)$$

whence

$$h^0 = (u^0 - c)^2. \quad (42)$$

Of course, $c=0$ for the stationary waves which will interest us. Therefore we take $c=0$ and combine (42) with the condition of geostrophic balance (36) to obtain

$$u^0 = K - \frac{f}{2}y, \quad (43)$$

where K is a constant. This is the condition on the mean flow which allows stationary nondispersive generalized Kelvin waves. It is a solvability condition from the first-order asymptotics. We will continue with an expansion for the rotating forced-dissipative system in the following section.

It is interesting to see the cross-channel structure of these linear solutions. Integration of (40) yields

$$H(y) = H(0)\exp\left(\int_0^y \frac{f}{u^0 - c}\right). \quad (44)$$

The Kelvin wave on a motionless background has $u^0=0$, c the square root of the background depth, and an exponential decay of strength away from the boundary. In contrast, these nondispersive solutions which live on a geostrophically balanced background flow have the integrand

$$\frac{f}{u^0 - c} = \frac{f}{K - c - (f/2)y}.$$

The cross-channel structure is algebraic. In fact, putting in $U=K-(f/2)y$, we obtain

$$H(y) = H(0)\left(1 - \frac{f}{2(K-c)}y\right)^{-2}. \quad (45)$$

For stationary waves, the strength of the perturbation grows from $y=0$ to $y=1$. These might be thought of as Kelvin waves propagating upstream on the boundary $y=1$ at just the right speed to balance advection.

The results are valid as long as $u^0 - c$ is single signed. If not, the integrals diverge, and the asymptotic theory is not uniformly well ordered. Since $(u^0 - c)^2 = h^0$, it is clear that the condition for the asymptotic theory to be valid is that the depth should not fall to zero. Rotation should not be so strong as to cause separated flow.

VI. ASYMPTOTIC BALANCE BETWEEN WIND STRESS AND SHOCKS: WEAK ROTATION

Now that the existence of nondispersive waves has been demonstrated, we set up the full asymptotic problem. We therefore replace

$$u \leftarrow u^0(y) + \epsilon u + \epsilon^2 u^2 + O(\epsilon^3),$$

$$v \leftarrow \epsilon^2 v + O(\epsilon^3),$$

$$h \leftarrow h^0(y) + \epsilon h + \epsilon^2 h^2 + O(\epsilon^3),$$

$$T \leftarrow \epsilon^2 T,$$

$$w \leftarrow \epsilon^3 w.$$

We have suppressed superscripts for the most frequently appearing variables in the forthcoming computations. Some of the computations have already appeared in the preceding section: for example, the zero-order balance is (36)

$$f u^0 = -h_y^0.$$

With the solvability condition $h^0 = (u^0)^2$ which results from taking the first-order equations, one has again

$$u^0 = K - \frac{f}{2} y.$$

In fact, we can take the entire set (37)–(39) with $v=0$ as the first-order equations. This time, we are concerned with the stationary states:

$$u^0(y) u_x = -h_x, \quad (46)$$

$$f u = -h_y, \quad (47)$$

$$u^0(y) h_x + h^0(y) u_x = 0. \quad (48)$$

From the first equation, we conclude that

$$u(x, y) = -\frac{1}{u^0(y)} h(x, y) + \frac{d(y)}{f},$$

where $d(y)$ is an arbitrary function of y . The general solution of (47) is then

$$h(x, y) = \exp\left(\int_0^y \frac{f}{u^0}\right) \left[\int_0^y \exp\left(-\int_0^s \frac{f}{u^0}\right) d(s) ds + \mathcal{L}(x) \right]. \quad (49)$$

The remainder of the work is in determining the constant of integration K , the two unknown functions $\mathcal{L}(x)$ and $d(y)$, and the location of the shock. The procedure is largely analogous to that of Sec. IV A. For example, the constant K comes from the total mass condition. Taking the total mass again to be N ,

$$N = \int_0^N \int_0^1 \left(K - \frac{f}{2} y\right)^2 dy dx = N \left(K^2 - \frac{f}{2} K + \frac{f^2}{12}\right).$$

For $u^0 > 0$, we choose the positive root of the quadratic

$$K = \frac{f}{4} + \sqrt{1 - \frac{f^2}{48}}. \quad (50)$$

Applying the method of Sec. IV A to the second-order equations gives

$$\mathcal{L}(x) = -\frac{C}{B} \pm \frac{1}{B} \sqrt{2AB[T_m - T(x)]}, \quad (51)$$

with

$$A = \left(K - \frac{f}{2}\right)^{-1}, \quad (52)$$

$$B = \frac{6}{7} \frac{1}{K^2 f} \left[\left(1 - \frac{f}{2K}\right)^{-7} - 1 \right], \quad (53)$$

$$C = 3 \int_0^1 \left(1 - \frac{fy}{2K}\right)^{-5} (u^0)^{-3} \int_0^y \left(1 - \frac{fs}{2K}\right)^2 d(s) ds dy + \int_0^1 \frac{2}{f} \left(1 - \frac{fy}{2K}\right)^{-3} \frac{d(y)}{(u^0)^2} dy. \quad (54)$$

Specifically, in computing (51), we took the second-order equations. Multiplication of the x -momentum equation by u^0 and subtraction of the continuity equation gives

$$(u^0 u^2 - h^2)_t + u^0 u_y v - h^0 v_y = -u^0 \left(\frac{u^2}{2} + T\right)_x + (hu)_x.$$

Upon multiplication by the integrating factor $(1 - fy/2K)^{-1}$ and integration from $y=0$ to $y=1$, the terms in v^2 vanish, yielding

$$\frac{d}{dt} \int_0^1 \left(1 - \frac{fs}{2K}\right)^{-1} (u^0 u^2 - h^2) dy = \int_0^1 \left(1 - \frac{fs}{2K}\right)^{-1} \left(\frac{T_x}{u^0} + \frac{uu_x}{u^0} - \frac{(hu)_x}{h^0}\right) dy.$$

The right-hand side must be zero in order not to produce secular solutions. The solvability condition is

$$0 = \int_0^1 \left(1 - \frac{fs}{2K}\right)^{-1} \left(\frac{T_x}{u^0} + \frac{uu_x}{u^0} - \frac{(hu)_x}{h^0}\right) dy.$$

We can substitute for u its expression in terms of h , then substitute (49), and finally integrate to obtain

$$0 = AT_x + B\mathcal{L}\mathcal{L}_x + C\mathcal{L}_x, \quad (55)$$

where A, B, C are as above. The remainder of the procedure—determination of $\mathcal{L}(x)$ from $T(x)$ —mimics Sec. IV A.

It is shown in the Appendix that $d(y)$ reduces to a constant d_0 by enforcing mass and momentum conservation at the shock at second order. The expression for C then simplifies to

$$C = \frac{2K}{3f} d_0 B. \quad (56)$$

With this result in hand, we can recompute $h(x, y)$ [cf. (49)],

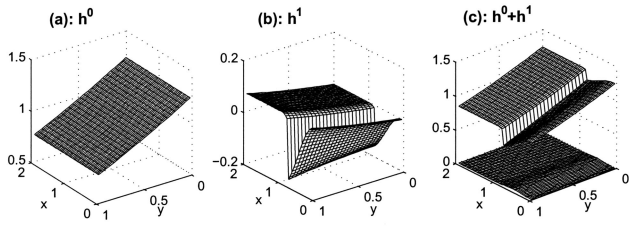


FIG. 4. Asymptotics, moderate rotation. $f=0.5$, $T_m=0.02$, $w=0.001$, $\epsilon=0.14$. (a) The zero-order solution. (b) The first-order solution. (c) The sum of the zero-order and first-order solutions. The bottom topography is just visible.

$$h(x,y) = -d_0 \left(\frac{2K}{3f} \right) \left(1 - \frac{fy}{2K} \right) \pm \left(1 - \frac{fy}{2K} \right)^{-2} \sqrt{\frac{2A}{B}} \sqrt{T_m - T(x)}. \quad (57)$$

The value of d_0 follows by demanding that the perturbation mass has integral zero (the topography is a second-order quantity),

$$d_0 = \frac{6f}{f-4K} \frac{2K}{f-2K} \sqrt{\frac{2A}{B}} \frac{1}{N} \left[\int_{x_j}^{x_m} \sqrt{T_m - T(x)} dx - \int_{x_m}^{x_j} \sqrt{T_m - T(x)} dx \right]. \quad (58)$$

The shock location x_s may be had by balancing wind stress and form drag or energy input and dissipation. For example, we have the steady-state x -momentum equation, integrated over the entire channel,

$$\int_0^N \int_0^1 \left(hu u + \frac{h^2}{2} \right)_x + (huv)_y + fhv \, dy \, dx = \int_0^N \int_0^1 -hT_x + w \, dy \, dx.$$

Since $\iint fhv \, dy \, dx = 0$ in a steady state, the only remaining balance is between the two integrated terms on the right, just as in (20). Computing this balance at third order gives

$$wN = \frac{4}{3} \frac{2K}{2K-f} \sqrt{\frac{2A}{B}} [T_m - T(x_s)]^{3/2}. \quad (59)$$

Figure 4 shows a plot of the asymptotic solution for the depth over weak topography with weak rotation. The first panel is a plot of the zero-order solution h^0 , the second panel shows the first-order perturbation h , and the last panel shows the combination. In particular, the perturbation shows the algebraic increase in shock strength with cross-channel coordinate which is due to the unusual structure of the nondispersive Kelvin wave. The bottom topography is just visible in the last panel.

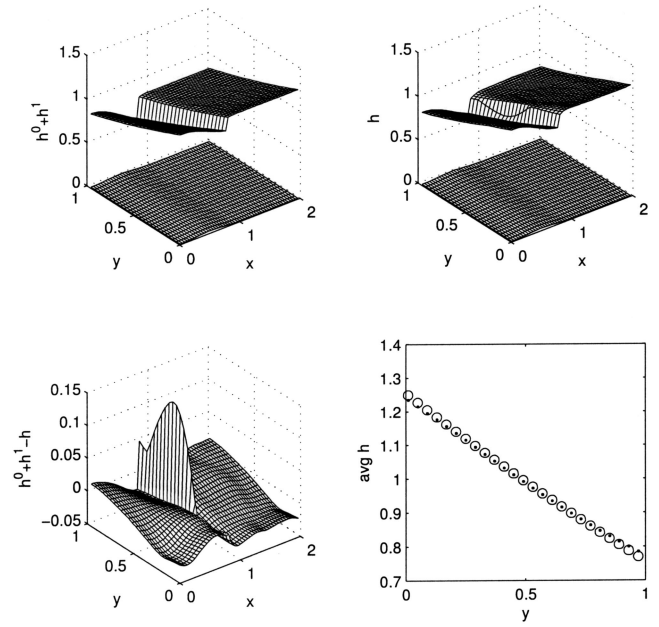


FIG. 5. Asymptotics, moderate rotation. $f=0.5$, $T_m=0.02$, $w=0.001$, $\epsilon=0.14$. (UL) Asymptotic prediction and topography, (UR) numerical solution and topography, (LL) difference, (LR) along-channel averaged depths. (Dots are numerics, circles are asymptotics.) The numerics are plotted at reduced resolution in this and subsequent figures; see comments in Sec. IX.

VII. COMPARISON OF NUMERICAL SOLUTION WITH ASYMPTOTICS

A shock-resolving Godunov-type numerical method (Sec. IX) was used to integrate the SWE from stationary initial conditions to the stationary shock. This was accomplished first by performing the integration without rotation, and then gradually increasing the rotation to the desired amount. Figure 5 compares the asymptotic solution pictured

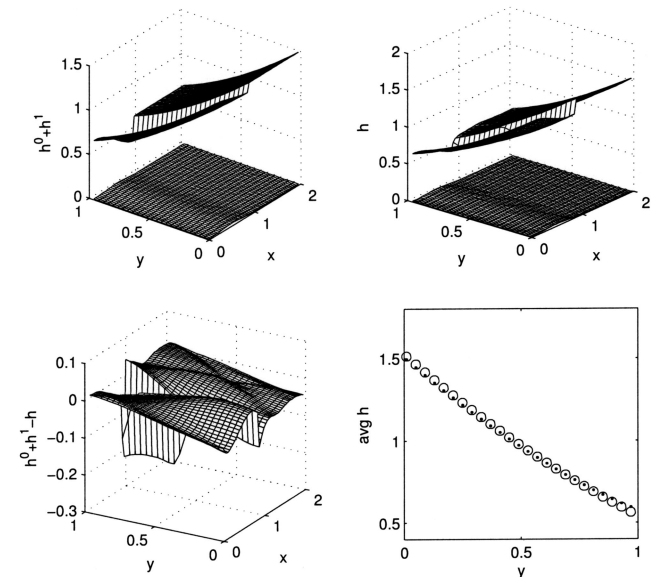


FIG. 6. Asymptotics, moderate rotation. $f=1.0$, $T_m=0.02$, $w=0.001$, $\epsilon=0.14$. (UL) Asymptotic prediction and topography, (UR) numerical solution and topography, (LL) difference, (LR) along-channel averaged depths. (Dots are numerics, circles are asymptotics.)

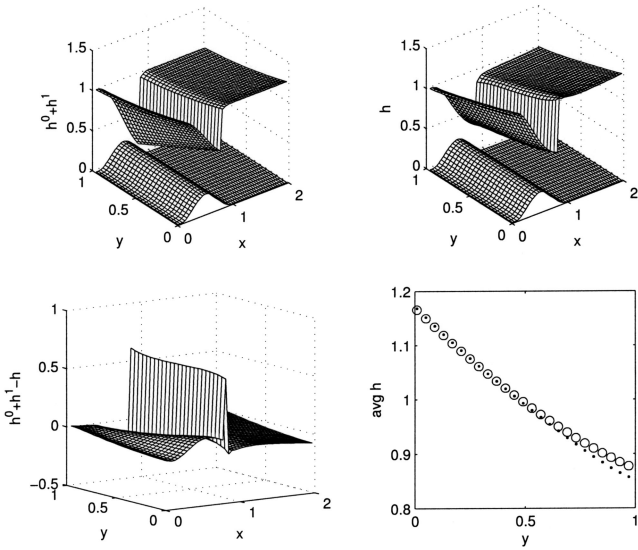


FIG. 7. Asymptotics, moderate rotation. $f=0.5$, $T_m=0.25$, $w=0.044$, $\epsilon=0.5$. (UL) Asymptotic prediction and topography, (UR) numerical solution and topography, (LL) difference, (LR) along-channel averaged depths. (Dots are numerics, circles are asymptotics.)

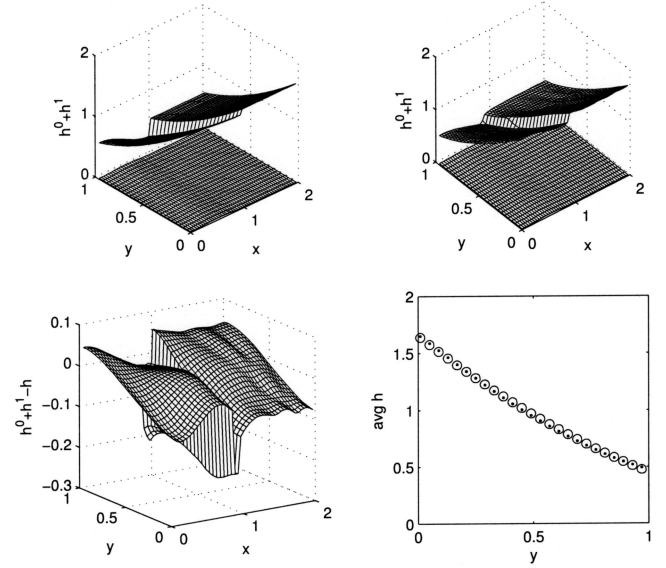


FIG. 8. Asymptotics, moderate rotation. $f=1.232$ asymptotics, $f=1.25$ numerics, $T_m=0.02$, $w=0.001$, $\epsilon=0.14$. (UL) Asymptotic prediction, (UR) numerical solution and bottom topography, (LL) difference, (LR) along-channel averaged depths. (Dots are numerics, circles are asymptotics.)

in Fig. 4 with the numerical solution for the same parameters. The agreement is quite good. Figure 5 also shows the along-channel depth averages of the numerical result against the zero-order asymptotic prediction, and the difference in the depth fields over the mesh. Agreement for the velocity fields is similar. Interestingly, the pronounced cross-channel increase in the asymptotic shock strength is not clearly present in the numerical solutions. It is not certain why this occurs. It is possible that carrying the asymptotics to higher order would reduce the discrepancy.

Part of the disagreement in the first-order field is due to a slight misalignment of the shock between asymptotics and numerics. Even misalignment by a single grid cell or numerical smearing over a few grid cells can give rise to locally large errors, but the error is otherwise $O(\epsilon^2)$.

Excellent agreement between the asymptotics and the numerics for the x -averaged depth field carries on to larger values of f , even as the local differences between asymptotic prediction and numerical result grow (Fig. 6). This even holds for substantially larger topographies: case $\epsilon=0.5$ is Fig. 7.

For further increase in the rotation, asymptotic predictions can no longer be calculated, because they predict that

the wind stress is too great for a steady state with the given topography. We take as an example the case for which $b_m=0.02$, $w=0.001$, and the largest possible asymptotic rotation is $f=1.2325$ [(59); see also Sec. VII A]. Figure 8 shows the largest prediction which is possible to obtain asymptotically along with a numerical experiment which converged just beyond the range of the asymptotics.

It is possible to compare energy dissipation at the shock with the energy input from the wind stress using the formula (14) and the energy input rate

$$\int_0^1 \int_0^N wu \, dx \, dy.$$

For several reasons, such comparisons are imperfect. It is not possible to determine exactly which jumps in the numerical data are due to the shock, and which are part of the natural discontinuity of the numerical method (Sec. IX). However, because of the cubic dependence of the energy dissipation on shock strength, this is not a major concern as long as the shock location is approximately captured. A more serious problem is that it is difficult to determine precisely which values should be taken as the before-shock and after-shock

TABLE I. Energy input and removal rates for several numerical integrations to a stationary state.

f	w	T_m	Wind input rate ($\times 10^{-3}$)	Shock dissipation rate ($\times 10^{-3}$)
0.0	0.001	0.02	1.76	1.60
0.5	0.001	0.02	1.77	1.52
1.0	0.001	0.02	1.82	1.73
1.25	0.001	0.02	1.83	1.56
0.0	0.044	0.25	56.7	57.3
0.5	0.044	0.25	58.0	61.0
1.0	0.044	0.25	72.0	70.7

depths and velocities. We have attempted to minimize the error by working with high-resolution methods. The energy input and shock dissipation are seen to be comparable in all cases. Table I compares energy input and energy output estimates in a few instances.

The assumption that the cross-channel velocity v is $O(\epsilon^2)$ was found to be valid for all numerical experiments shown in this section. This means that the numerical experiments show essentially the same general features as the asymptotic solutions. In particular, ageostrophic boundary layers are weak and the shocks show little curvature from the wall at $y=0$ to the wall at $y=1$. Shock curvature can be checked for visually in Figs. 5–8 by looking for mesh lines parallel to the y axis which cross the shock. Only in Fig. 8, computed near the limiting wind stress for which the theory can be applied, is shock curvature significant.

A. Maximal wind stress

We have found that for a given topographic maximum and rotation, there is a maximum allowable wind stress [(59) with $T(x_j)=0.0$]. We checked this in a few cases with numerical simulations, but the number of checks was limited by the time cost of the numerical experiments (Sec. IX). With $f=0.5$ and $T_m=0.02$, the asymptotic maximal wind stress is $w=0.00134$. Numerical runs with the slightly greater wind stress $w=0.0014$ were observed to converge to a steady state, whereas $w=0.0016$ ran away. Likewise, with $f=0.5$ and $T_m=0.25$, the asymptotic maximal wind stress is $w=0.0591$. Numerical simulations with $w=0.044$ were observed to converge to a steady state, whereas $w=0.064$ ran away.

VIII. STRONG ROTATION

We cannot use asymptotics to discuss stationary forced-dissipative flow after separation of the flow from the wall $y=1$ because such methods fail when the mean depth is zero somewhere in the domain. However, we found in a few numerical simulations that for a given wind stress, the shock separates from the left-hand side of the channel as the rotation is increased. There is a regime of rotation for which a steady state is reached, but if rotation is increased further, the flow eventually becomes supercritical everywhere and runs away. We were able to produce partially or fully separated steady shock patterns when ϵ was 0.71 ($f=3.0, 4.0$). It is not clear whether it is possible to achieve separated stationary flow for smaller ϵ ; no numerical simulations converged for smaller ϵ with strong rotation. Possibly strong nonlinearity of the flow is necessary.

In Figs. 9–14 are shown streamlines, depth fields, and velocity fields of some of these separated flow solutions. There is typically an extremely shallow ($h < 10^{-3}$) flow leftwards of the shock and the shock-associated flow field. (This corresponds approximately to the region in which $\ln(h) < -6$ in the pseudocolor plots in Figs. 9 and 12.) In a steady state, this shallow region appears to interact very weakly with the separated shock pattern. The total mass and momentum content of the extremely shallow region is typically less than 10^{-4} of the total mass and momentum.

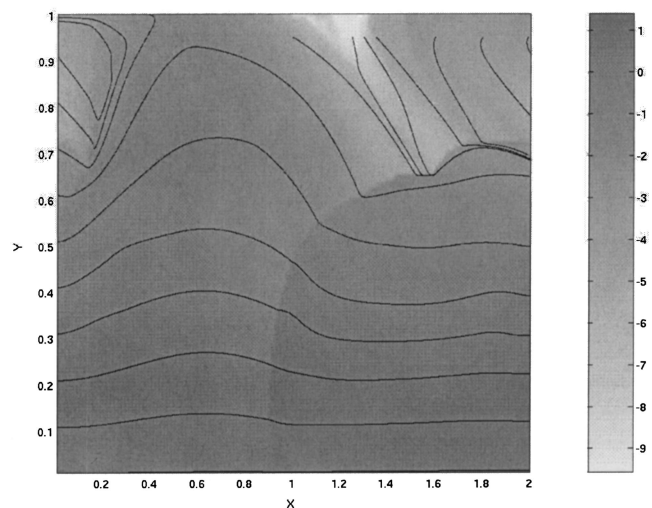


FIG. 9. Streamlines and column depth. $f=3.0$, $T_m=0.5$, $w=0.1$. The pseudocolor scale on the right shows the natural logarithm of the thickness of the fluid column h .

Possibly, the extremely shallow flow is a numerical artifact which arises from the treatment of extremely shallow cells in the numerical method (Sec. IX). The shock pattern itself also contains a rather shallow flow on its leftward margin, but as can be seen in the figures, the flux of momentum in the shallow flow is necessary to maintain the shock at its left edge.

The most prominent features of the separated shock pattern are the curvature of the shock at its leftward extreme and the recurrence of shocking waves downstream of the primary shock. Fedorov and Melville predicted the curvature of a rotating shock away from a boundary in a half plane under assumptions of weak cross-channel flow and propagation into constant-depth fluid.⁴ Those assumptions are not valid in these simulations, but the result is nevertheless suggestive.

The intriguing recurrence suggested an experiment in which the length of the domain was doubled ($N=4$), with the expectation that additional periods of recurrence would ap-

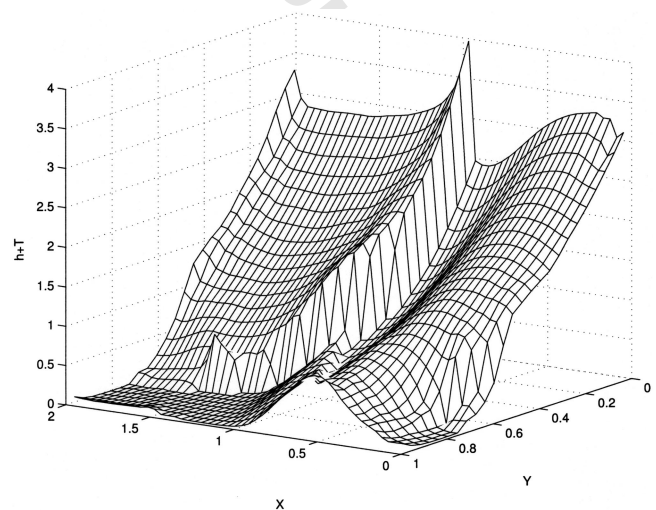


FIG. 10. Free surface. $f=3.0$, $T_m=0.5$, $w=0.1$.

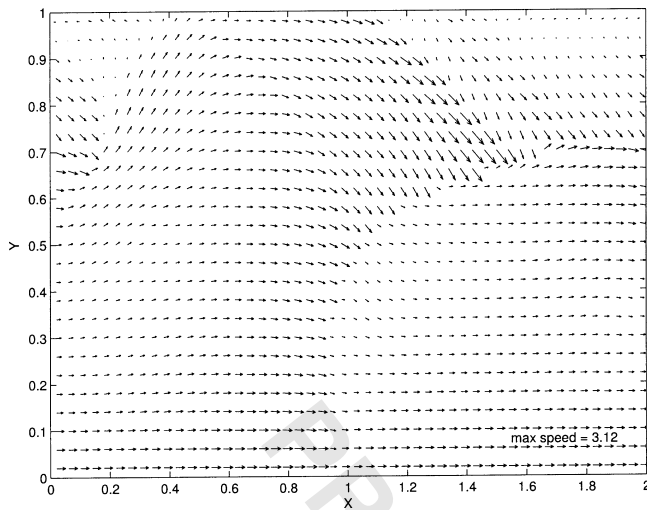


FIG. 11. Velocity field. $f=3.0$, $T_m=0.5$, $w=0.1$.

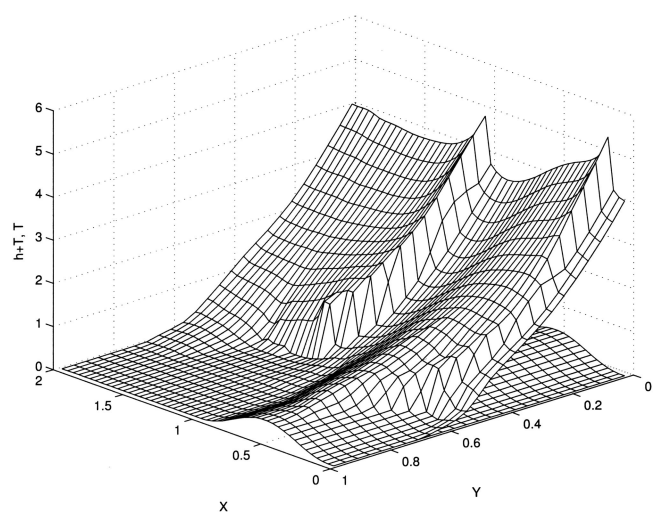


FIG. 13. Free surface and topography. $f=4.0$, $T_m=0.5$, $w=0.1$.

pear in the stationary state. However, none of these numerical experiments were observed to converge to a steady state. Because of the long times required to establish a steady state in such a situation (even from nearby steady states with weaker rotation it takes several days on the computers at Courant), this may be a consequence of an inability to tune the parameters in the experiment rather than an indication that such states do not exist. At the same time, this may indicate that the stationary states observed for strong rotation are rather sensitive objects.

The separated solutions were produced by taking un-separated steady solutions, increasing the rotation rate, and allowing the flow to come to equilibrium. All of the separated solutions described in this section showed no appreciable variation in the flow field over a period of at least 10^3 nondimensional time units (which is at least an order of magnitude larger than the forcing time scale). This period corresponds to $O(10^3)$ advective transits of the periodic domain.

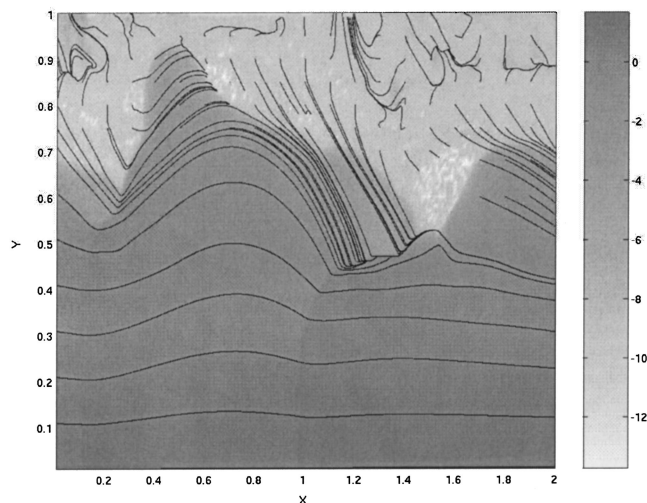


FIG. 12. Streamlines and column depth. $f=4.0$, $T_m=0.5$, $w=0.1$. The pseudocolor scale on the right shows the natural logarithm of the thickness of the fluid column h .

IX. NUMERICS

In order to properly resolve shocks, a hand-built second-order (in space and time) Godunov-type shallow water solver was used. The incorporated Riemann solver was based on following the exact Riemann invariants of the SWE along characteristics.¹⁴ The Riemann solver was modified to give an exact solution of the Riemann problem in the case that one of the states has zero depth. This is easily done since the wave propagating into the dry cell must be a rarefaction. Verifications were performed for one- and two-dimensional dam-break problems onto dry land. The two-dimensional simulations were performed both parallel to the grid and at an angle to check for anisotropy. Run-up onto a dry plane beach, for which exact Riemann invariants exist, was checked by diagnosing the conservation of these invariants along characteristics. (For unit slope, the Riemann invariants are found to be $u \pm 2\sqrt{h+t}$.)

Second-order Strang splitting of the x and y dimensions and the forcing terms—including rotation—was used.¹⁵ Reflecting (wall) boundaries were implemented with ghost

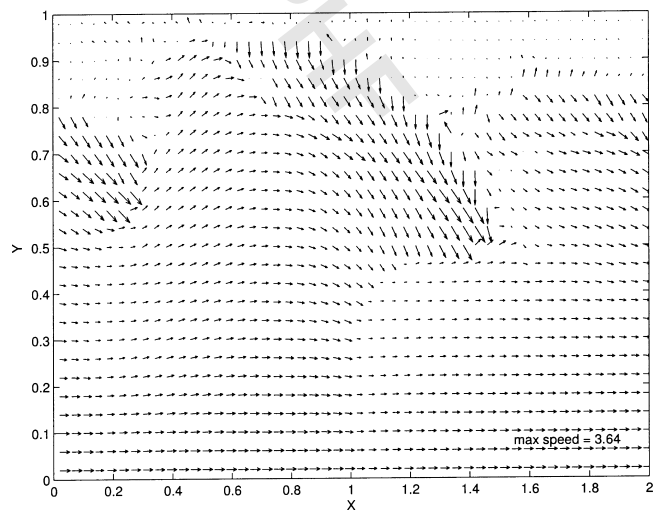


FIG. 14. Velocity field. $f=4.0$, $T_m=0.5$, $w=0.1$.

cells. These boundaries were only active during the y -update phase of the time splitting, since neither the along-channel phase nor the forcing phase is sensitive to the reflecting nature of these boundaries.

Explicit methods of this type are excellent at correctly resolving shocks. However, CFL conditions based on the maximum wavespeed make them expensive to run to forced-dissipative equilibrium. In some of the verification runs with weak topography and wind stress, the integration times for convergence to a steady state (even for perturbations from a nearby steady state) required several million time steps. All the integrations displayed in this paper were performed at a resolution of 100×200 . In order to test that the simulations were well resolved, trials at 200×400 were performed in a few cases; they compared well with the lower-resolution simulations. Simulations at 50×100 were also tried, and found to be inadequate. The figures in this chapter are interpolated data at the reduced resolutions 25×50 and 50×100 .

Two alterations to standard methods were made for the numerics in this paper. Both were made for the case in which the depth h of the fluid drops to zero. This case was investigated in Sec. VIII. The first alteration limits the wind stress as $h \rightarrow 0$. The wind stress forcing update is typically

$$u_t = w/h.$$

This leads to unreasonably large velocities for small h . This is not only undesirable from the point of view of the numerics, which are overwhelmed by the corresponding time step restrictions, but physically unrealistic as well. It is reasonable to believe that the magnitude of the velocity would in reality be limited by frictional effects and possibly by departure from shallow water behavior. Rather than try to build these into the model, we made the wind stress a function of h , as follows:

$$\tilde{w} = \begin{cases} w & \text{if } h > 0.1 \\ (19h - 0.9)w & \text{if } 0.1 \geq h > 0.05 \\ hw & \text{if } h \leq 0.05. \end{cases}$$

Even with this modification, the occasional shallow fluid cell ($h \leq 0.01$) was observed to achieve large velocities, probably due to splitting error. In this case, we did the simplest thing we could think of: the momentum was entirely removed from these offending cells. Also, cells with $h < 10^{-6}$ were reset to zero mass and momentum. The total mass and momentum truncation was recorded. Typical mass losses were less than one-thousandth of 1% of the total mass after 10^5 time steps. Typical momentum loss per unit time was less than one-thousandth of 1% of the momentum added by the wind stress per unit time.

These limiting modifications took effect only when extremely shallow fluid cells appeared—a case which was limited to separation or near-separation from the wall $y=1$.

X. CONCLUDING REMARKS

Although the asymptotic theory performs admirably for weak to moderate rotation, it cannot be applied to flows which are sufficiently strong as to cause separation from the

left wall. The difficulty is not only the additional complication of a free boundary, but also the vanishing depth field, which can no longer be considered to be $O(1)$ throughout the flow.

In the numerical simulations of strong rotation, the region of the flow near the free boundary hardly resembles the linearly nondispersive asymptotic flow structure. However, away from the free boundary, the structure remains. In view of this, one may conjecture that even the wall at $y=0$, which is not present in many geophysical applications, may not be required either. Suppose that the wall was removed, and the region $y < 0$ was replaced with a different zonal flow in geostrophic balance; as an illustrative example, rather than $(u^0)^2 = h^0$, we might have $u^0 = 0$, $h^0 = \text{const}$. The extension of the wave field into this region would be dispersive, but it is not obviously necessary that this would destroy the nondispersive nature of the flow for $y > 0$. Indeed, one could argue that maintenance of a nondispersive flow region is favored if there is to be a forced-dissipative steady state.

Of course, the existence of such a free generalized Kelvin wave would require forcing conditions maintaining the mean flow which are different from the cross-channel-uniform forcing of this paper. It is unclear whether the global structure would be amenable to asymptotic treatment, but such nonuniform forcing is certainly relevant to geophysical research.

APPENDIX: d_0 IS CONSTANT

Because the asymptotic solution involves a weak solution, we must be careful to ensure that the correct conservation laws are obeyed at the shock. Use of the smooth PDE to handle the asymptotics away from the shock does not guarantee this, but we have the freedom to do so in the undetermined function $d(y)$. Specifically, we determine $d(y)$ by demanding that mass and momentum fluxes are continuous at the shock at all orders. The fluxes are

$$h_T u_T = (h^0 + \epsilon h + \epsilon^2 h^2)(u^0 + \epsilon u + \epsilon^2 u^2) = h^0 u^0 + \epsilon(h^0 u^0 + u^0 h) + \epsilon^2(hu^0 + h^0 u^2 + u^0 h^2), \quad (\text{A1a})$$

$$h_T u_T u_T + \frac{h_T^2}{2} = (h^0 + \epsilon h + \epsilon^2 h^2)(u^0 + \epsilon u + \epsilon^2 u^2)^2 + \frac{1}{2}(h^0 + \epsilon h + \epsilon^2 h^2)^2 = h^0 u^0 u^0 + \frac{1}{2}(h^0)^2 + \epsilon[(u^0)^2 h + 2u^0 h^0 u + 2h^0 h] + \epsilon^2 \left[2u^0 h^0 u^2 + h^0 u^2 + 2u^0 h u + (u^0)^2 h^2 + h^0 h^2 + \frac{1}{2}h^2 \right]. \quad (\text{A1b})$$

We have used the subscript T (h_T , etc.) to indicate the total. No additional information is gained at zeroth order, and the order 1 conditions are the same as those derived in Sec. VI. However, at second order

$$[hu] = -[h^0 u^2 + u^0 h^2], \quad (\text{A2a})$$

$$\left[h^0 u^2 + 2u^0 h u + \frac{1}{2} h^2 \right] = -[2u^0 h^0 u^2 + (u^0)^2 h^2 + h^0 h^2], \quad (\text{A2b})$$

where the brackets indicate the jump across the shock. The second equation may be simplified, since $(u^0)^2 = h^0$, meanwhile multiplying the first equation by $2u^0$,

$$[2u^0 h u] = -[2u^0 h^0 u^2 + 2(u^0)^2 h^2],$$

$$\left[h^0 u^2 + 2u^0 h u + \frac{1}{2} h^2 \right] = -[2u^0 h^0 u^2 + 2h^0 h^2].$$

A difference of the equations yields

$$\left[h^0 u^2 + \frac{1}{2} h^2 \right] = 0$$

and substitution of $u = -h/u^0 - d(y)/f$ makes

$$\frac{3}{2} [h^2] = -2 \frac{h^0 d(y)}{u^0 f} [h].$$

Since $[h^2] = (h_l + h_r)[h]$,

$$d(y) = -\frac{3 u^0}{2 h^0 f} \frac{h_l + h_r}{2}.$$

Substitute the expression (49) to get

$$d(y) = -\frac{3 u^0}{2 h^0 f} \left(1 - \frac{f}{2\kappa} y\right)^{-2} \left[\int_0^y \left(1 - \frac{f}{2\kappa} s\right)^2 d(s) ds + \frac{\mathcal{L}_l + \mathcal{L}_r}{2} \right].$$

We have derived the integral equation

$$\left(1 - \frac{f}{2\kappa} y\right)^2 \frac{u^0}{f} d(y) = -\frac{3}{2} \left[\int_0^y \left(1 - \frac{f}{2\kappa} s\right)^2 d(s) ds - \frac{C}{B} \right]. \quad (\text{A3})$$

Let

$$l(y) = \left(1 - \frac{f}{2\kappa} y\right)^2 d(y),$$

and differentiate (A3) by y to obtain

$$\left(l(y) \frac{u^0(y)}{f} \right)_y = -\frac{3}{2} l(y).$$

Remembering that $u_y^0 = -f/2$,

$$\frac{u^0}{f} l_y = -l. \quad (\text{A4})$$

This equation may be integrated to find that

$$l(y) = d_0 \left(1 - \frac{f}{2\kappa} y\right)^2,$$

or that

$$d(y) = d_0,$$

where d_0 is a constant.

¹O. Bühler and T. E. Jacobson, "Wave-driven currents and vortex dynamics on barred beaches," *J. Fluid Mech.* **449**, 313 (2001).

²A. E. Gill, "The hydraulics of rotating channel flow," *J. Fluid Mech.* **80**, 641 (1977).

³D. Nof, "Geostrophic shock waves," *J. Phys. Oceanogr.* **16**, 886 (1986).

⁴A. V. Fedorov and W. K. Melville, "Hydraulic jumps at boundaries in rotating fluids," *J. Fluid Mech.* **324**, 55 (1996).

⁵K.R. Helfrich *et al.*, "Nonlinear Rossby adjustment in a channel," *J. Fluid Mech.* **390**, 187 (1999).

⁶L. J. Pratt *et al.*, "Hydraulic adjustment to an obstacle in a rotating channel," *J. Fluid Mech.* **404**, 117 (2000).

⁷M. S. Goldak, Form drag in wind-driven ocean flows, Ph.D. thesis, New York University, 1998.

⁸G. K. Batchelor, *An Introduction to Fluid Dynamics* (Cambridge University Press, New York, 1967).

⁹B. Cushman-Roisin, *Introduction to Geophysical Fluid Dynamics* (Prentice-Hall, Englewood Cliffs, 1994).

¹⁰A. E. Gill, *Atmosphere-Ocean Dynamics* (Academic, New York, 1982).

¹¹R. Salmon, *Lectures on Geophysical Fluid Dynamics* (Oxford University Press, New York, 1998).

¹²G. B. Whitham, *Linear and Nonlinear Waves* (Wiley, New York, 1974).

¹³D. J. Acheson, *Elementary Fluid Mechanics*, (Clarendon, Oxford, 1990).

¹⁴E. G. Tabak, A second-order Godunov method on arbitrary grids, *J. Comput. Phys.* **124**, 383 (1996).

¹⁵R. J. LeVeque, *Numerical Methods for Conservation Laws* (Birkhauser, Boston, 1992).